Available online at www.CivileJournal.org

Civil Engineering Journal

(E-ISSN: 2476-3055; ISSN: 2676-6957)

Vol. 10, No. 08, August, 2024

Retrofitting Bolted Flange Plate (BFP) Connections Using Haunches and Extended End-Plates

Budi Suswanto [1*], Fikri Ghifari [2], Yuyun Tajunnisa [3], Data Iranata [1]

[1] *Department of Civil Engineering, Institut Teknologi Sepuluh Nopember (ITS), Surabaya, Indonesia.*

[2] *Ph.D Student of Civil and Construction Engineering, National Taiwan University of Science and Technology (NTUST), Taipei, Taiwan.*

[3] *Department of Civil Infrastructure Engineering, Institut Teknologi Sepuluh Nopember (ITS), Surabaya, Indonesia.*

Received 30 April 2024; Revised 17 July 2024; Accepted 23 July 2024; Published 01 August 2024

Abstract

In Indonesia, one of the most common forms of connection is the Bolted Flange Plate (BFP) moment connection. Nevertheless, their current setups do not satisfy the strict requirements outlined in AISC 358-22. Therefore, this study uses advanced sub-assemblage numerical modeling simulations using ANSYS software to propose a novel way to integrate a half WF extended end-plate connection and trapezoidal haunch in order to fortify BFP moment connections, which does not meet the requirement required by AISC 358-22. Methodologically, the research entails comprehensive modeling and analysis of the proposed retrofit scheme. Six distinct connection models were scrutinized: the BFP-UR representing the existing connection extracted from a structure in Surabaya; the BFP-R4E and BFP-R4ES models, embodying connection retrofits with a half WF extended end-plate; and the BFP-RTR and BFP-RSTR models, embodying connection retrofits with a trapezoidal haunch. Additionally, the BFP-RTRE model integrates both an extended end plate and a trapezoidal haunch in the retrofit scheme. The analytical findings unveil that the proposed strengthening paradigm manifests heightened and superior rotational moment characteristics relative to the pre-reinforcement configuration, albeit encountering stiffness degradation attributable to buckling effects on the main beam. Notably, the analysis indicates that degradation ensues when rotational displacement exceeds 4%, with only the BFP-RTR and BFP-RSTR models exhibiting degradation at a 3% rotation threshold. Crucially, the connections demonstrate the capability to withstand 80% of the beam's plastic moment under a 4% rotational displacement, thereby aligning with the stringent requisites delineated in AISC 341-22.

Keywords: Retrofitting of Moment Connections; Bolted Flange Plate; Prequalified Connections; Finite Element Method; Connection Capacity.

1. Introduction

The Northridge earthquake in 1994 caused the moment steel frame structure to fall in America, shedding light on the fact that while steel materials are highly ductile, they may also display brittleness if not properly specified. The reason for the failure was the welded flange-bolted web connection's poor ability to absorb seismic energy [1]. The Los Angeles Department of Building and Safety has detected the following damages, as follows [2]:

- The weld connection cracks and subsequently propagates to the column flange.
- Cracks occur due to the heat-affected zone (HAZ) phenomenon.
- The composite action of the concrete slab with the beam induces a disparity between the position of the neutral axis under a positive moment (composite structure) and that under a negative moment (non-composite structure), leading to axial deformation of the lower fiber beam flange and resulting in fracture.

* Corresponding author: budi_suswanto@its.ac.id

http://dx.doi.org/10.28991/CEJ-2024-010-08-03

After the Northridge earthquake, efforts to further retrofitting research continued, especially with regard to reinforcement at beam-column connections. A suggestion put out by Uang and Bondad aims to improve the performance of welded flange-bolted web joints by adding a triangular haunch [3]. Four damaged connections were the focus of full-scale tests under both static and dynamic loads as part of the investigation. The findings showed that strengthening the broken connections with a triangular haunch improves their functionality and moves the plastic hinge away from the column face, focusing all of the stress on the beam. After that, a haunch was added to the damaged specimens, and they were put through additional testing. The results of the static and dynamic tests showed a significant improvement in the cyclic performance, especially after some adjustments were made to the top flange's groove-welded joint, which ensures that the plastic hinging of the beam happens away from the column face. Saberi et al. [4]: Six susceptible bolted T-Stub connections were strengthened using a triangular haunch and subjected to cyclic loading conditions in an experimental setting. The results show that adding haunches to the strengthening could potentially cause the production of plastic hinges on the beam instead of bolt failure or yielding on the T-Stub flange. Furthermore, after being reinforced with welded haunches, the connections' moment capacity and rotational stiffness increased. Experimental research has shown that this method can be applied to convert pinned connections into moment connections, as well as to repair bolted T-stub connections with weak flanges or weak bolts. The findings reveal that this strategy has potential for the rehabilitation of neighboring simply braced frames with insufficient space between them.

Saberi et al. furthered the development of strengthening using a triangular haunch by utilizing one on two end-plate weak connection specimens that underwent cyclic loading in an experimental setting. The acquired result suggests a change in the failure mechanisms from yielding at the end-plate or bolt failure to the development of plastic hinges on the beam elements [5]. Shi et al. [6] carried out an experimental investigation to determine how the height of the triangular haunch affected the area of the defective panel zone, which did not match the design specifications. The study's findings showed that the panel zone area has strong ductility and produces a sizable amount of plastic deformation. Moreover, it was discovered that the panel zone's rigidity and loading capacity were improved by the addition of the triangle haunch. Asada et al. [7] by using bolts as connecting elements between the strengthening and pre-existing connection elements, the horizontal haunch was further improved. Testing with cyclic loads was applied to this adjusted arrangement. The results showed that plastic hinges developed in the horizontal haunch region rather than the existing connecting area. As a result, the beam flange experienced local buckling. D'Aniello et al. proposed trapezoid haunch dampers with free form damage (FREEDAM) [8] to investigate the effectiveness of the haunch as the dampers of the connection. The first yield is shifted to the beam at the tip of the haunch when FREEDAM is present. Additionally, Richards & Lee suggested using horizontal shear-yielding haunches as a damper [9].

The horizontal shear-yielding haunches increase the high post-yield rigidity by 10-15%. The benefit of steel haunches is also applied in the retrofit of RC beam-column connections, as demonstrated by the work of Sahil et al. [10]. The ductile failure of the beam-column connections has replaced the brittle failure caused by the steel haunches. Additionally, the beam-column capacity has improved by up to 89% thanks to the steel haunches. Zhang et al. [11] investigated the effect of the triangular haunch numerically on the existing extended end-plate. It can be determined that the triangular haunch only marginally improves strength—only 5% more than the current connection—and causes a greater decrease in stiffness because of local buckling at the haunch's tip. Its 12% increase in energy dissipation makes it the greatest, though. Qiao et al. [12] examined the impact of the reinforced flange plate on the steel beam that was connected to the opening-column. The connection's failure mode changed from beam-end cracking to web-opening cracking when the reinforced plate connection was present. Additionally, when compared to an unreinforced connection, the connection strength is also greatly boosted.

The extended end-plate connection consists of a plate that is welded to the end of the beam and then attached to the column and beam. It was Sumner et al. who suggested this relationship [13] and then used as one of the prequalified connections [14]. Solhmirzaei et al. [15] created a unique panel zone design for the extended end-plate connection, using channel steel in place of the traditional doubler and continuity plates. Experimental testing revealed that this novel structure exhibits a notable 36% increase in ductility and 25% higher energy dissipation when compared to traditional extended end-plate connections. Yilmaz et al. [16] carried out an experimental investigation to evaluate the differences in performance between the bolted flange plate type connection (BFP-01) and the extended end-plate type connection (BSEP-01). According to the test results, the moment capacity generated by the BFP-01 connection was 257.4 kN-m, but the moment capacity generated by the BSEP-01 connection was 281.8 kN-m.

In Indonesia, a connection that is frequently utilized is the Bolted Flange Plate (BFP) moment connection, as shown in Figure 1. In order to avoid brittle failure, this link adheres to a hierarchy of failures. The bolt slippage is the first step, and then the beam at the connection plate's end yields. At some point, the flange plate itself will yield [17]. Because of their small architectural footprint and ease of implementation, BFP connections are highly preferred. It is important to keep in mind, too, that the BFP connections that are now in use in Indonesia are usually quite thin—often less than 16 mm—and are meant to be used in earthquake-resistant constructions. In spite of this, BFP connections fall under the category of prequalified connections and are governed by ANSI/AISC 358-22 [18]. Restricting the flange plate's yielding and any possible yielding during large deformations is the desired behavior of BFP connections during earthquakes. Thus, it is essential that the flange plate be thick enough to bear significant deformations without breaking.

Figure 1. Bolted Flange Plate (BFP) moment connection

This study's goal is to assess the current BFP moment connection in accordance with AISC 358-22's requirements. After that, a numerical analysis is done to look into how the current BFP moment connection behaves. By adding horizontal haunches and expanded end-plates, five retrofitting models have been proposed to improve the current BFP moment connection, which does not adhere to AISC 358-22. The majority of previous studies have mostly concentrated on using either horizontal or welded triangular haunches. Moreover, a number of studies have examined the behavior of retrofitting specimens or models using pre-Northridge connections as their specimens or models. Even though AISC 358-22 regulates BFP moment connections, it's noteworthy that a sizable percentage of BFP moment connections that are now in place in Indonesia do not comply with according to AISC 358-22, the probable maximum moment at the location of a plastic hinge, M_{pr} (kN-m), can be calculated as follows:

$$M_{pr} = C_{pr} R_y f_y Z_e \tag{1}$$

$$C_{pr} = \frac{f_y + f_u}{2 f_y} \leq 1.2 \tag{2}$$

where C_{pr} is a factor to account for peak strength, R_y is a ratio of the expected yield stress to the design yield stress, Z_e is an effective plastic section modulus at the location of a plastic hinge (mm^3), f_y is the design yield stress (MPa), and f_u is the ultimate stress (MPa), for design purposes, the required moment, M_f (kN-m), was taken from the face of the column and can be calculated as:

$$M_f = M_{pr} + V_p S_h \tag{3}$$

$$S_h = S_1 + s\left(\frac{n}{2} - 1\right) \tag{4}$$

where V_p is the shear forces located at the plastic hinge location (kN), S_h is the plastic hinge location (mm), S_1 is the distance from the face of the column to the nearest bolt (mm), and s the bolt's spacing (mm), n is the bolt's number. The definition of the plastic hinge location can be seen in Figure 2. Since the BFP connection transforms the moment force into the axial couple forces $\left(F_{pr}\right)$, the axial couple force can be analyzed as:

$$F_{pr} = \frac{M_f}{(d + t_n)} \tag{5}$$

where d is the beam's depth and t_p is the flange plate's thickness (mm). To ensure that the BFP connection can resist the required axial couple force, the tensile rupture strength, the tensile yielding strength, and the shear block strength should be greater than the required axial couple force.

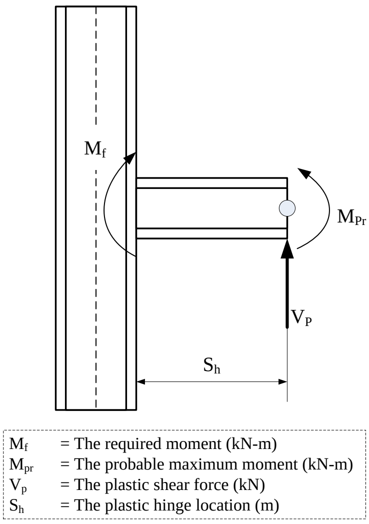

Figure 2. Definition of S_h [2]

2. Analysis Procedure

The general research flow is presented in Figure 3. At the beginning, the existing BFP connection is analyzed by using a linear elastic perfectly plastic analysis in order to evaluate the strength of the existing BFP based on AISC 358-22. The non-linear analysis is performed if the existing BFP connection does not satisfy the required strength. The acceptance criteria of the non-linear analysis are that the connection could resist the 80% beam's plastic moment at a rotation of 4% [19]. Moreover, the behavior and seismic capacity of retrofitting models are evaluated when the existing BFP connection does not meet the acceptance criteria that required by AISC 358-22.

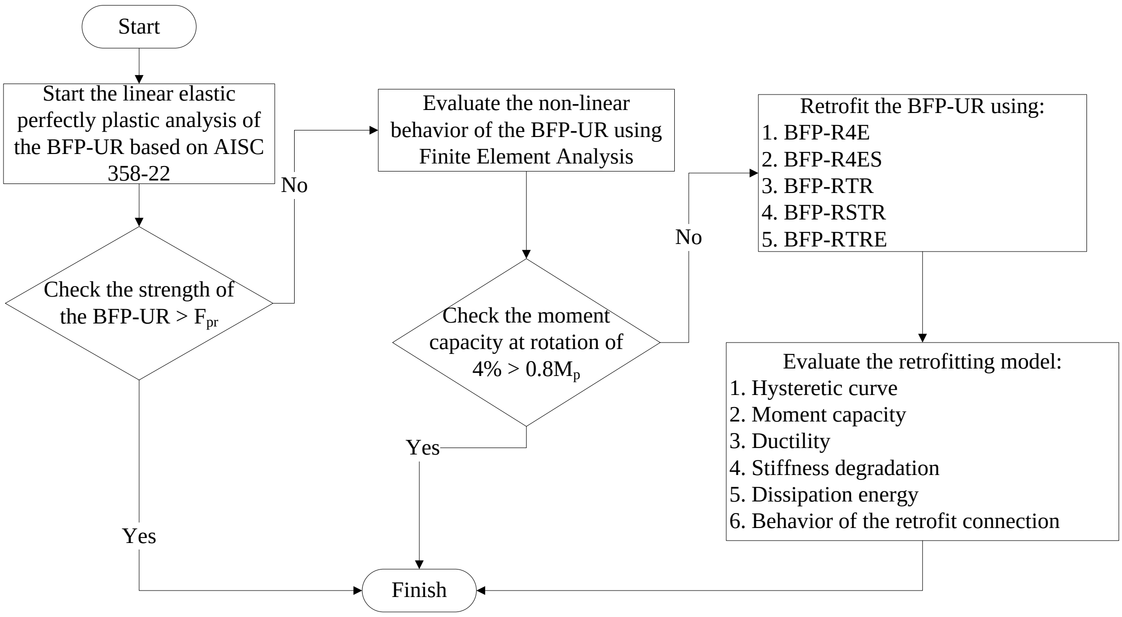

Figure 3. General research flow

2.1. Model and Material Properties

The connection models encompass a total of six configurations. The first model, designated as BFP-UR (unretrofitted), represents the existing connection prior to any reinforcement. The second and third models entail connections strengthened through the integration of both a horizontal haunch and an extended end-plate. Conversely, the fourth and fifth models involve Retrofitting with a combination of trapezoidal haunches and end-plates. Notably, the distinction between the second and third models lies in the absence of a stiffener at the end-plate for the second model (BFP-R4E), while the third model (BFP-R4ES) incorporates a stiffener at the end-plate. Similarly, the differentiation between the fourth and fifth models rests on the presence of a stiffener on the end-plate for the fifth model (BFP-RSTR), whereas the fourth model (BFP-RTR) remains unstiffened. Finally, the sixth model integrates a trapezoidal haunch with an extended end-plate (BFP-RTRE). These six connections will be modeled as sub-assemblages, with the dimensions of beams and columns determined in accordance with the research conducted by Yilmaz et al. [16].

In this research, the model comprises H250x250 H-beam columns, WF300x150 beams, and a haunch made from WF300x150 for Retrofitting purposes. Plates, including the flange plate, stiffener, end-plate, gusset, and continuity plate, are constructed from ASTM-A36 steel. Existing bolts utilize High Strength Bolts with a diameter of 20 mm (M20) and ASTM-A325 specifications. Conversely, bolts for reinforcement employ high-strength bolts with a diameter of 20 mm (M20) and ASTM-A490 specifications. The stress-strain curve for ASTM-A36 steel is derived from the research conducted by Kang and Kim [20]. At the same time, the ASTM-A325 and ASTM-A490 were taken from the research of Kulak [21]. The summary of the model in this study is shown in Tables 1 and 2. The stress-strain curves are shown in Figure 4 to 6. The six research models are shown in Figures 7 to 12.

Table 1. Proposed model

Model	Column	Beam	Haunch	End-plate stiffener
BFP-UR			-	-
BFP-R4E				-
BFP-R4ES	Hbeam 250×250	WF300×150		Plate 10 mm
BFP-RTR			Ex-WF300×150	-
BFP-RSTR				Plate 10 mm
BFP-RTRE				-

Table 2. Material properties

Elements	Grade	Yield Stress, f_y (MPa)	Ultimate stress, f_u (MPa)	Ultimate elongation, ε_u (10^{-3})
Column	ASTM-A36	250	400	23.17 [20]
Beam				
Haunch				
Plate				
Existing Bolts	ASTM-A325	660	838.59	22.627 [21]
Retrofitting Bolts	ASTM-A490	942.69	1188.6	20.306 [21]

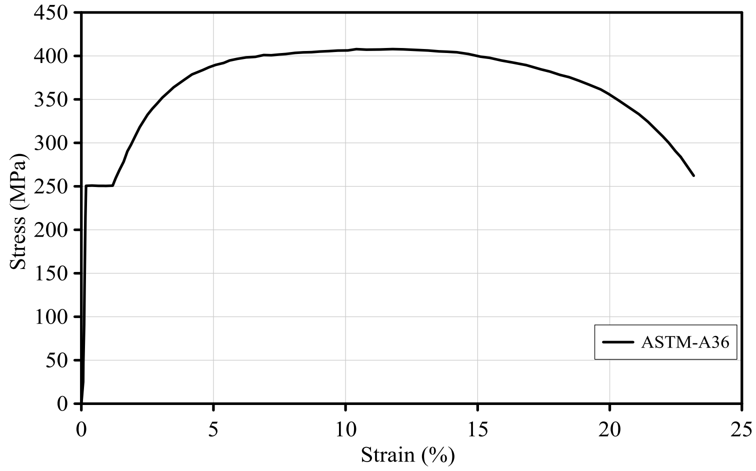

Figure 4. Stress-strain Curve of ASTM-A36 [20]

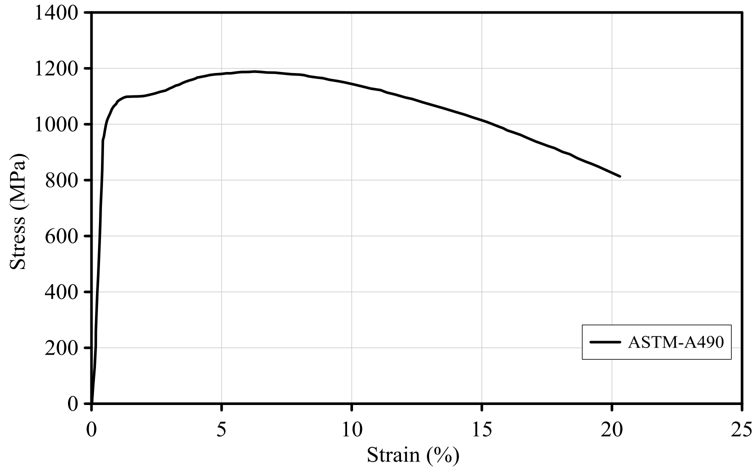

Figure 5. Stress-strain curve of ASTM-A490 [21]

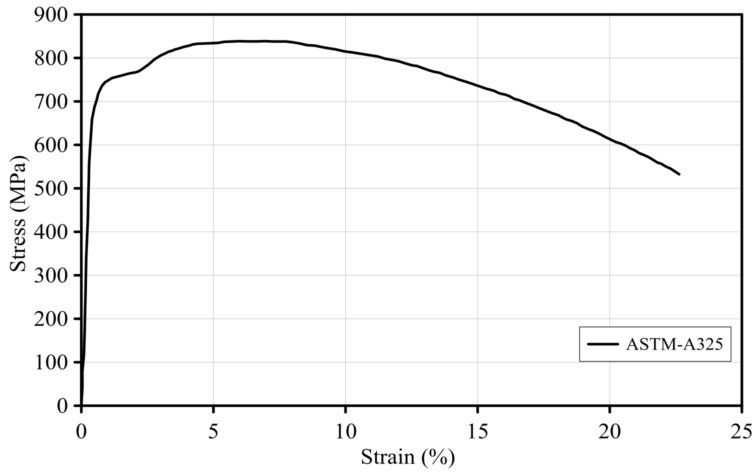

Figure 6. Stress-strain curve of ASTM-A325 [21]

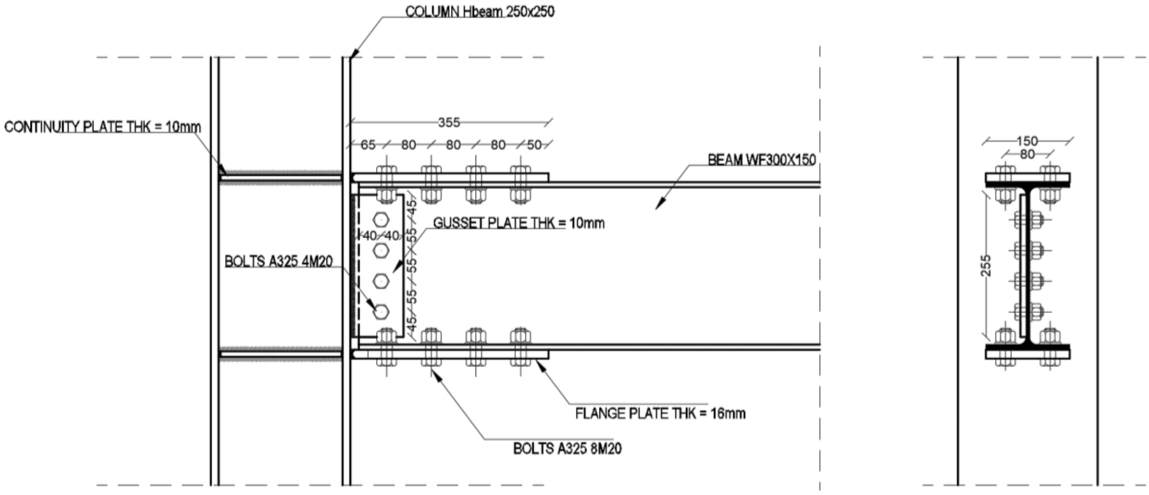

Figure 7. BFP-UR model (unit: mm)

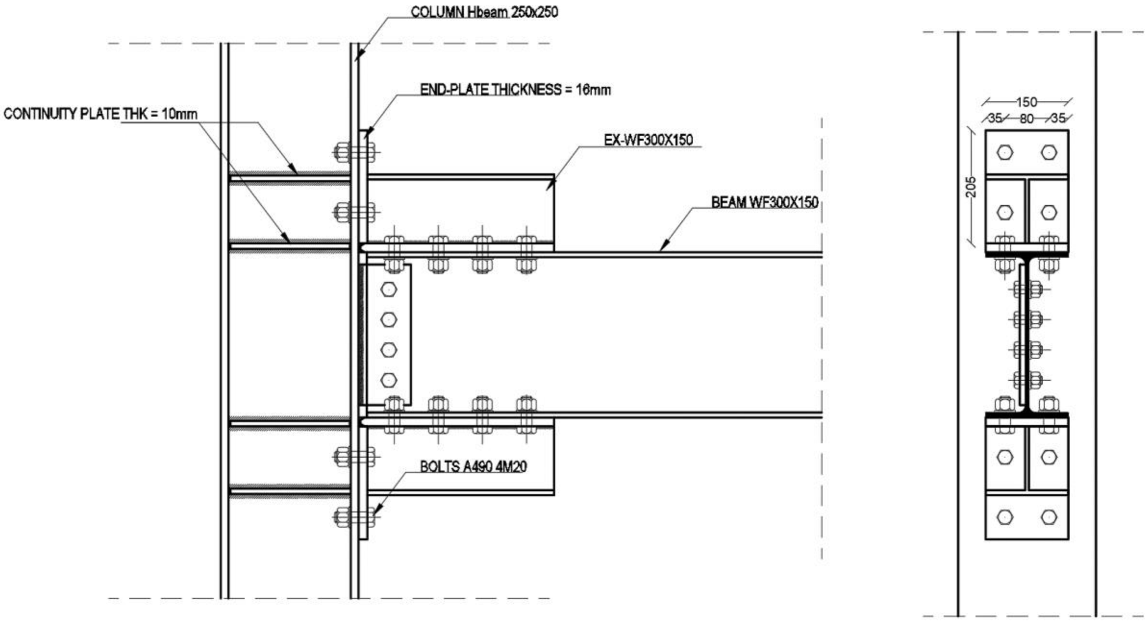

Figure 8. BFP-R4E model (unit: mm)

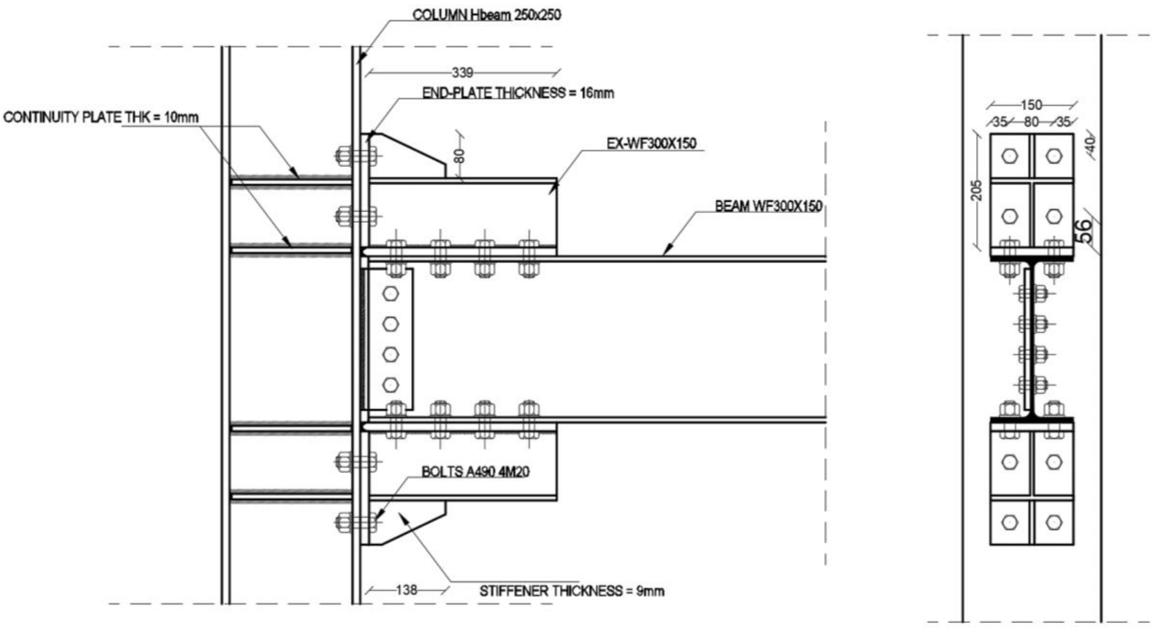

Figure 9. BFP-R4ES model (unit: mm)

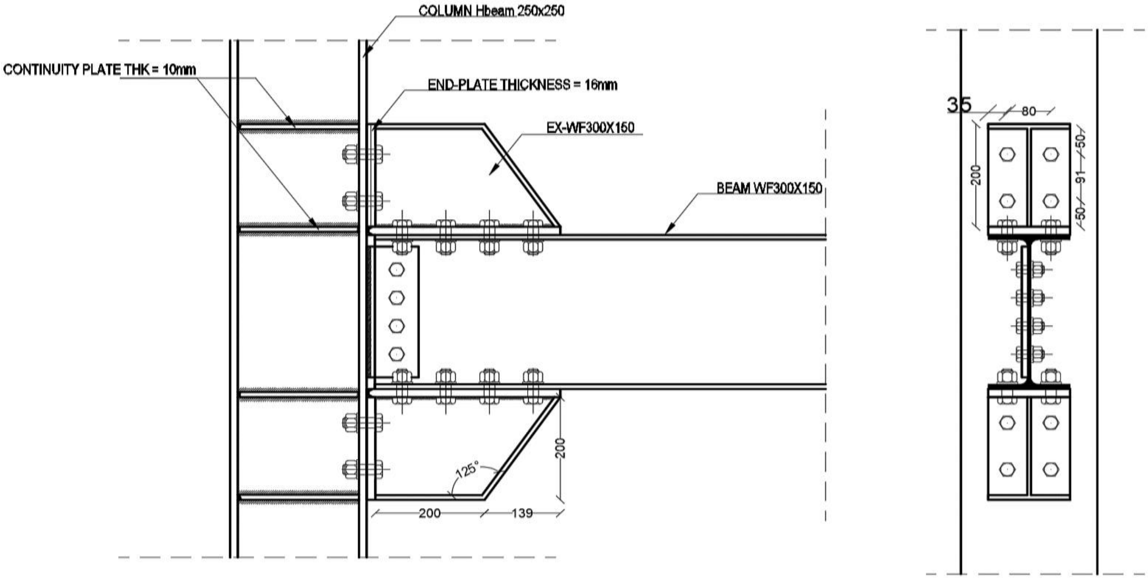

Figure 10. BFP-RTR model (unit: mm)

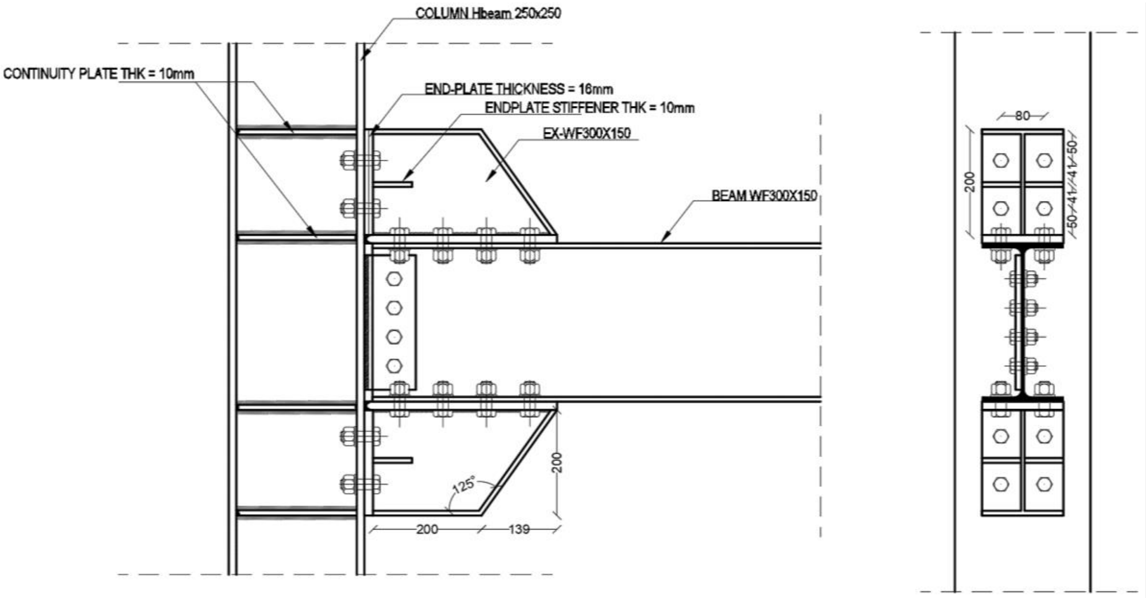

Figure 11. BFP-RSTR model (unit: mm)

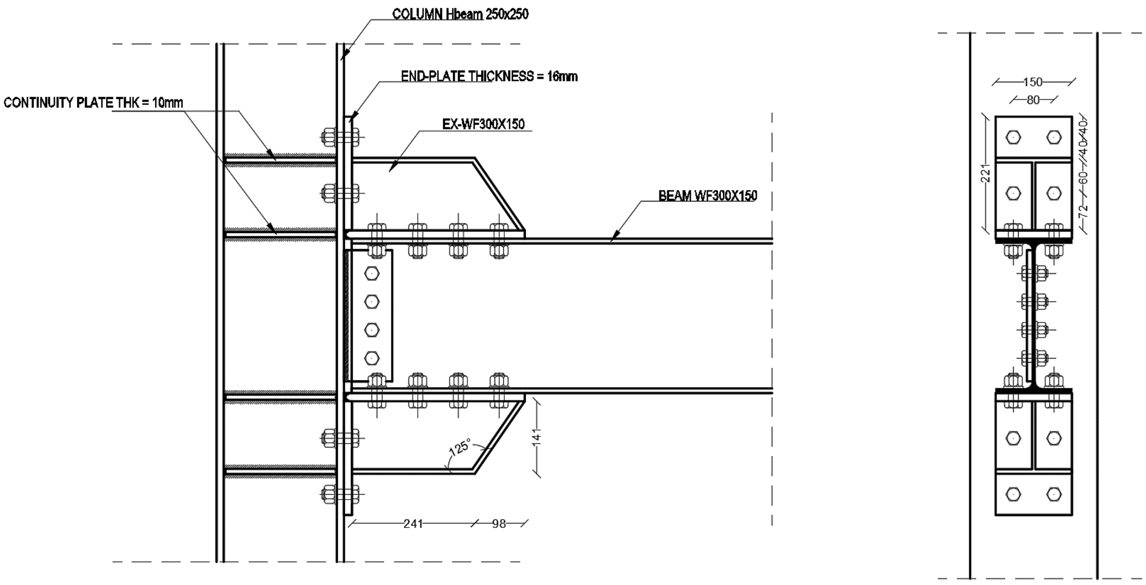

Figure 12. BFP-RTRE model (unit: mm)

2.2. Numerical Analysis Method

In this research, numerical analysis is conducted utilizing the ANSYS program. All models are represented using three eight-node brick elements (SOLID185), which constitute a solid three-dimensional model with eight nodes. Each node possesses three degrees of freedom [22]. The meshing technique employed in this research is hexahedral meshing, utilizing a multizone approach to automatically divide the structure into mapped zones [23]. The meshing dimensions used are 50 mm for the solid element without holes, 16 mm for the solid element with holes, and 8 mm for the bolts. The connections between structural elements are defined using bonded contact to represent welded connections, friction between bolts and plates with a frictional coefficient of 0.25, and frictionless contact between plates. All models are subjected to cyclic loading following the guidelines outlined in ANSI/AISC 341-16 [24] and FEMA 350 [25], as shown in Figure 13. The applied load is located at the tip of the beam in the direction of y-direction as shown in Figure 14. The imperfection condition is performed by running an Eigenvalue buckling analysis and the first mode is chosen to proceed the non-linear analysis. In addition, the large deflection analysis is chosen to consider the second order effect. The boundary condition of the column is set by using a remote displacement and behave as a hinge support, as shown in Figure 15-a. In order to prevent the beam from the Lateral Torsional Buckling (LTB), the lateral displacement of the beam is set to zero as shown in Figure 15-b.

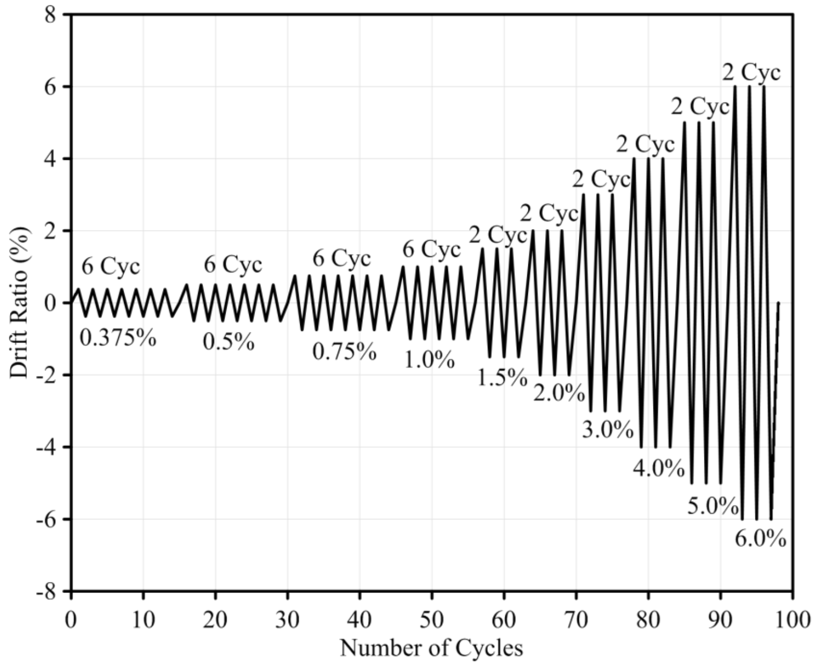

Figure 13. Cyclic loads history

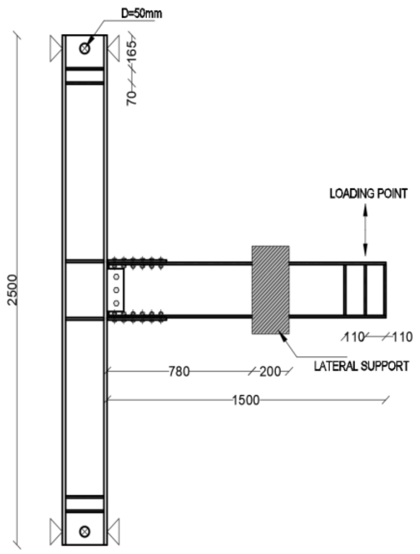

a) Sub assemblage system

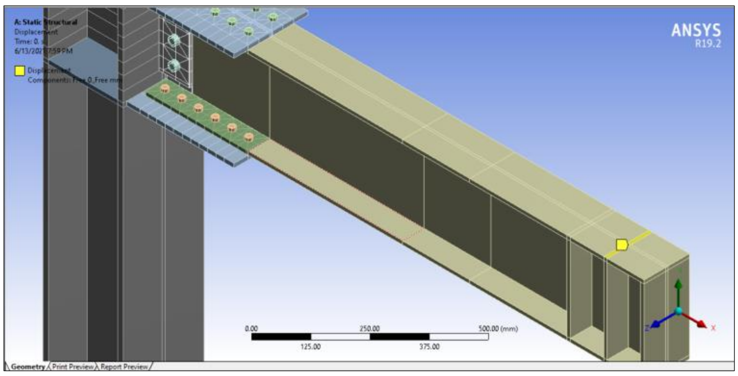

b) Location of the loading in the direction of u_3

Figure 14. Sub Assemblage configuration [16]

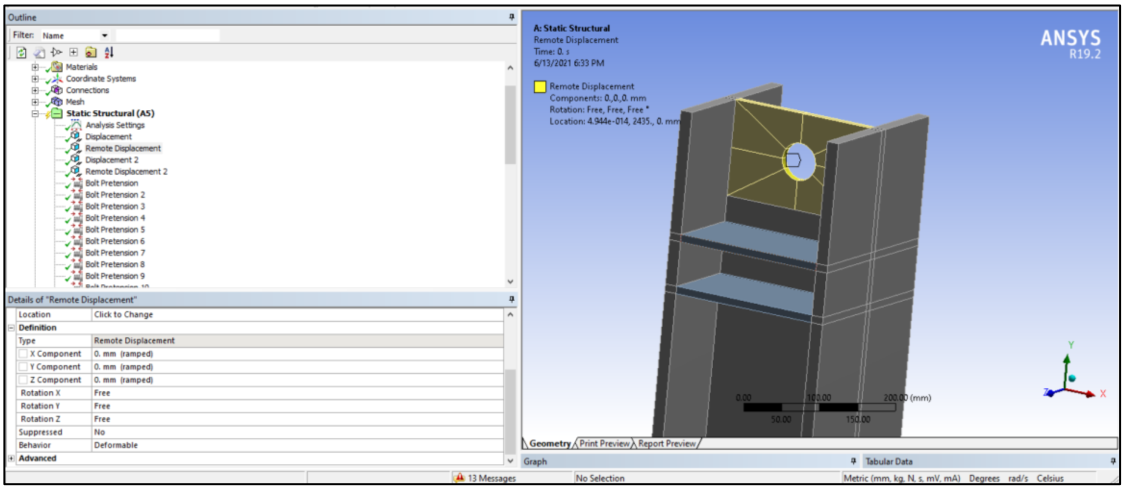

a) Remote displacement

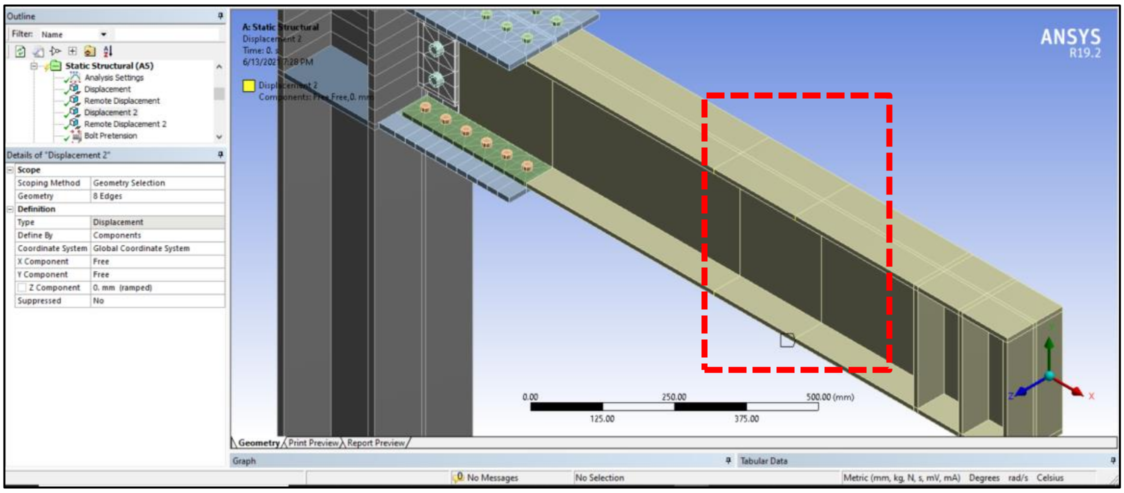

b) Displacement controlled

Figure 15. Boundary condition of the system

3. Results and Discussion

3.1. A linear elastic perfectly plastic analysis of the BFP-UR model

Before the numerical analysis is done using ANSYS, a linear elastic perfectly plastic analysis is the first step to analyze BFP connections according to ANSI/AISC 358-22 Section 7.6. The reduction factor used to calculate the strengths of the connection is 0.9 for the non-ductile element ($\emptyset_n$) and 1.0 for the ductile element ($\emptyset_d$). The result of the linear analysis is shown in Table 3. The result presents the capacity of the flange plate subjected to the axial couple force that has been calculated according to Equations 1 to 5.

Table 3. The linear analysis results

Strength Analysis	Capacity (kN)	Axial Couple Force, F_{pr} (kN)
Tensile yielding strength	600	
Tensile rupture strength	610.56	684.96
Shear block strength	1714.17	

The linear elastic perfectly plastic analysis indicates that the flange plates are unable to meet the required strength specified by ANSI/AISC 358-22. The tensile yielding strength and tensile rupture strength of the flange plate are insufficient to withstand the axial couple force. Consequently, a non-linear analysis will be conducted to observe the behavior of the connections. The non-linear analysis will focus on examining the moment-rotation curve, failure behavior, and stresses within the connection. Failure behavior will be assessed based on von Mises stresses occurring within the connection, while the moment capacity at the outer face of the column will be evaluated when the beam rotation reaches 0.04 radians, as per AISC 341-22 Section E3.6b. This section provides performance and design requirements for connections, with a special provision outlining criteria for the utilization of partially-restrained connections when supported by analysis justification.

3.2. Numerical Analysis Result

a. BFP-UR

Figure 16 illustrates a Hysteretic curve representing the correlation between moment and rotation, derived from the findings of the BFP-UR model. This curve is generated based on the deformation and force reactions observed at the tip of the beam, as depicted in Figure 13. Subsequently, these deformations and force reactions are transformed into rotation and moment values at the face of the column flange. At a beam rotation of 4% radians, the moment at the face of the column flange is measured at 165.47 kN-m, as indicated by the dot point in Figure 16. When comparing the BFP-UR model with 80% of the beam's plastic moment, the plastic moment is determined to be 173.16 kN-m. It yields a ratio of 1.046 between the 80% beam’s plastic moment and the moment capacity at the outer face of the column, which exceeds one.

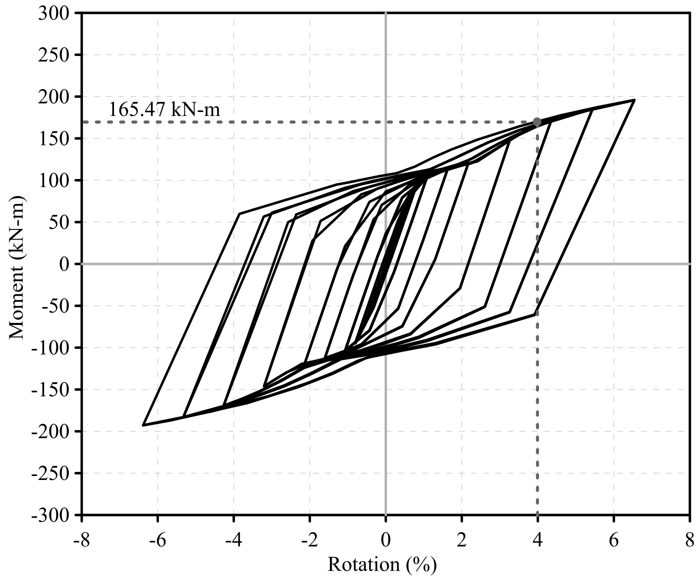

Figure 16. Hysteretic curve of BFP-UR model

The von Mises stress of the BFP-UR is shown in Figure 17. The first yield of the connection occurs at displacement of 7.5 mm and the location of the yielding is on the panel zone as shown in Figure 17-a. The stress magnitude of the first yield is 246.02 MPa. In this step, the beam is still on the elastic condition. At the end of the loading, the panel zone has the largest stress, which is 410 MPa and the yielding is formed at the beam, as shown in Figure 17-b. In addition, the connection between the flange plate and the flange column has a concentrated normal stress as shown in Figure 17-c. It indicates that the connection could not resist the stress as proven in the linear elastic perfectly plastic analysis.

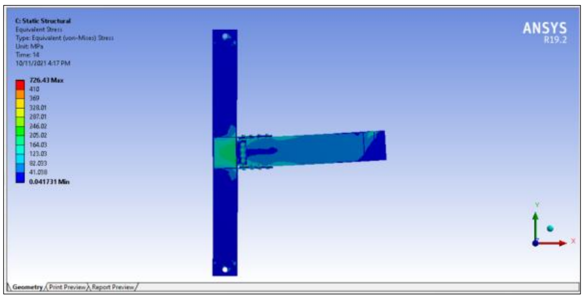

a) Yielding at displacement of 7.5 mm

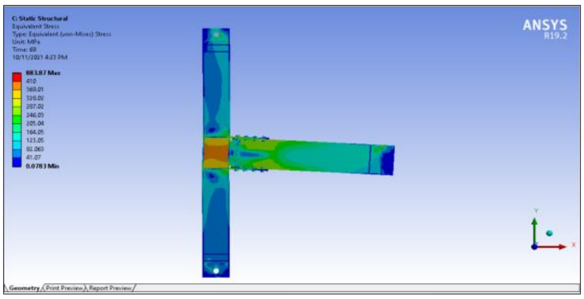

b) Ultimate at displacement of 90 mm

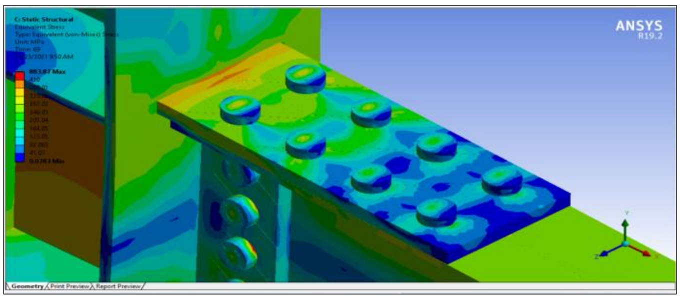

c) Stress on the flange connection at displacement of 90 mm

Figure 17. The von Mises stress of BFP-UR

b. BFP-R4E

Figure 18 displays a Hysteretic curve illustrating the relationship between moment and rotation at the face of the column for the BFP-R4E model. The present of the Retrofitting components results in a degradation of connection stiffness when rotation exceeds 4.36%. The maximum moment capacity achieved by BFP-R4E is 220.5 kN-m, while the moment capacity of BFP-R4E at a rotation of 4% is 210.667 kN-m, as indicated by the dot point in Figure 18. This represents an increase of 45.197 kN-m compared to the initial moment capacity. Notably, this exceeds the 80% plastic moment of the beam, which is 173.16 kN-m. The ratio between the 80% plastic moment of the beam and the moment capacity at rotation of 4% is 0.822. Consequently, it can be inferred that the Retrofitting model can effectively withstand the 80% plastic moment of the beam.

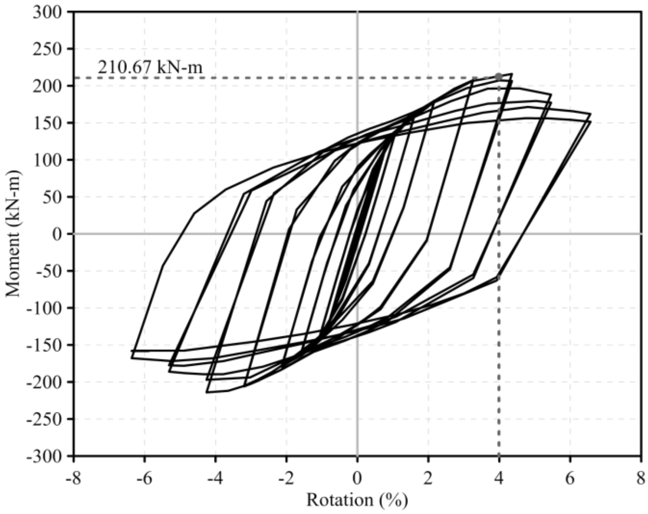

Figure 18. Hysteretic curve of BFP-R4E model

The von Mises stress of the BFP-R4E is shown in Figure 19. The first yield of the connection occurs at the displacement of 11.28 mm. Different from BFP-UR, the first yield occurs at the beam flange near the tip of the BFP connection as shown in Figure 19-a, with the stress magnitude of 256.28 MPa. The panel zone also experienced yielding although the majority of the panel zone is still in an elastic condition. At the same time, the end-plate also experienced a yielding at the intersection between the flange haunch and the end-plate as shown in Figure 19-b. This yielding occurs due to the insufficient of the end-plate thickness and lead to the prying-effect although the prying deformation is relatively small. At the end of the loading, the beam is buckling at the location where the first yield of the beam occurs as shown in Figure 19-c. The normal stress on the flange plate has reduced due to the presence of the horizontal haunch as shown in Figure 19-d.

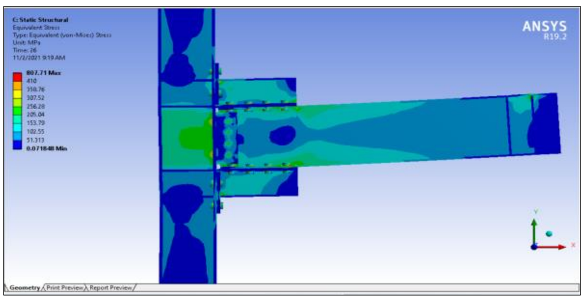

a) Yielding at displacement of 11.28 mm

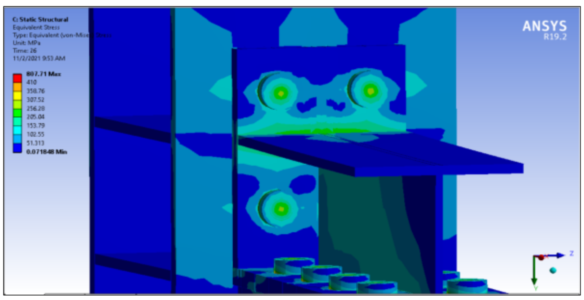

b) Stress on the end-plate at displacement of 11.28 mm

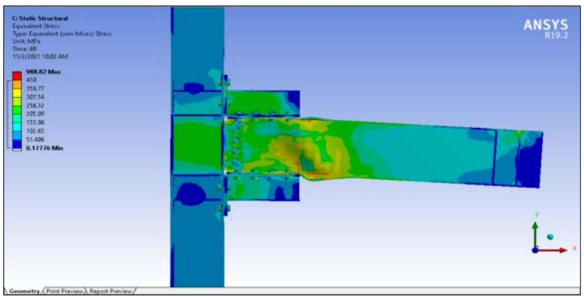

c) Ultimate at displacement of 90 mm

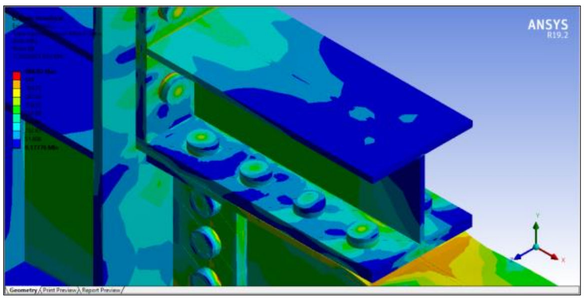

d) Stress on the flange connection at displacement of 90 mm

Figure 19. The von Mises stress of BFP-R4E

c. BFP-R4ES

The moment-rotation curve of the BFP-R4ES model at the face of the column is presented in Figure 20. The strength continues to experience degradation after a rotation of 4.35%, and the maximum moment that occurs before the stiffness degrades is 224.57 kN-m. When the rotation of 4% occurs, the connection produces a moment capacity of 214.02 kN-m, as shown in the data point on Figure 18. The moment capacity at rotation of 4% has exceeded 80% of the beam's plastic moment, which is 173.16 kN-m, with the ratio of 0.809, indicating its ability to resist the beam's plastic moment.

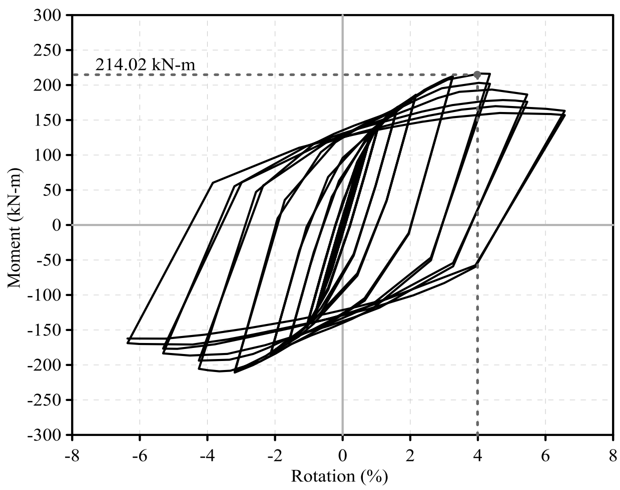

Figure 20. Hysteretic curve of BFP-R4ES model

The von Mises stress of the BFP-R4ES is shown in Figure 21. The first yield of the connection occurs at the displacement of 11.105 mm. The first yield occurs at the beam flange near the tip of the BFP connection as shown in Figure 21-a, with the stress magnitude of 246.04 MPa. Due to the presence of the stiffener, the panel zone experienced only a slight yielding. Compared to the BFP-R4E, the presence of the stiffener could resist the prying-effect effectively as shown in Figure 21-b. At the end of the loading, the beam is also buckling at the location where the first yield of the beam occurs as shown in Figure 21-c). The normal stress on the flange plate has reduced and similar to the BFP-R4E due to the presence of the horizontal haunch as shown in Figure 21-d.

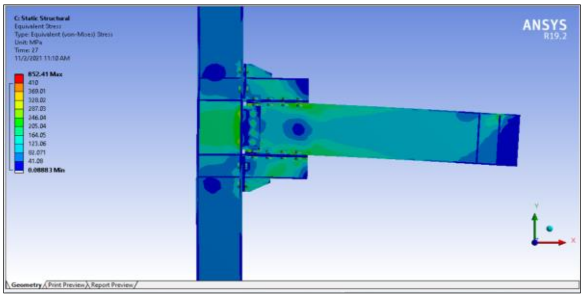

a) Yielding at displacement of 11.105 mm

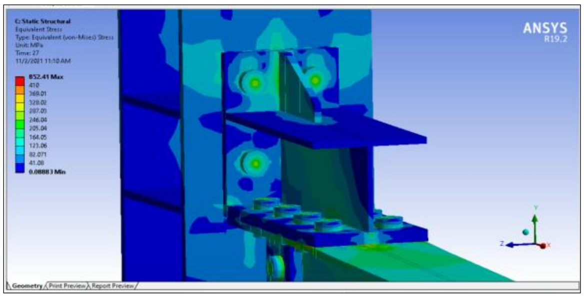

b) Stress on the end-plate at displacement of 11.105 mm

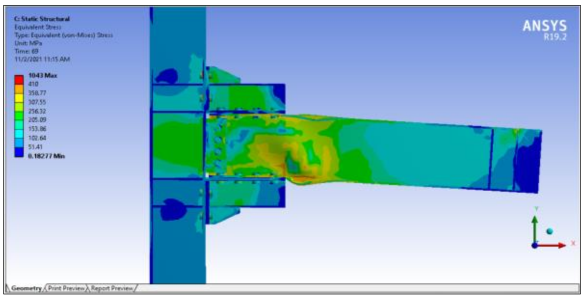

c) Ultimate at displacement of 90 mm

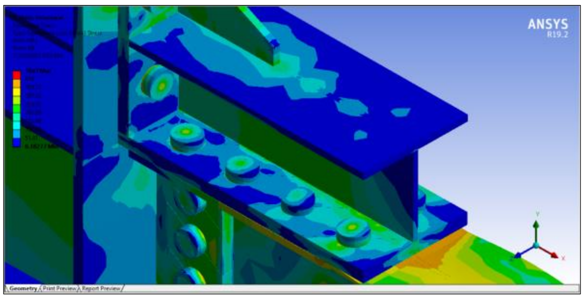

d) Stress on the flange connection at displacement of 90 mm

Figure 21. The von Mises stress of BFP-R4ES

d. BFP-RTR

The moment-rotation curve generated by the BFP-RTR model is depicted in Figure 22. This model yields a maximum moment of 216.9 kN-m before strength degradation occurs. At rotation of 4%, the model's moment capacity is 204.60 kN-m, which is 17.46 kN-m smaller than the average moment capacity of the BFP-R4E and BFP-R4ES models. Despite this difference, the moment capacity at 4% rotation still exceeds 80% of the beam's plastic moment, with a ratio of 0.85. Therefore, the model meets the prequalification requirements outlined by the AISC.

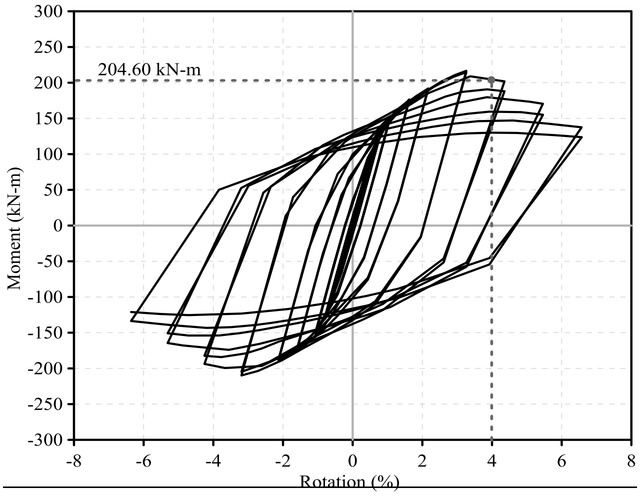

Figure 22. Hysteretic curve of BFP-RTR model

The von Mises stress of the BFP-RTR is shown in Figure 23. The first yield of the connection occurs at the displacement of 11.105 mm. The first yield occurs at the beam flange near the tip of the BFP connection as shown in Figure 23-a, with the stress magnitude of 246.03 MPa. The panel zone experienced only a slight yielding compared to the BFP-R4E with the stress magnitude of 205 MPa. It can be concluded that the retrofitting method could increase the area of the panel zone. Hence the stress of the panel zone is not only focused on the certain location. However, the trapezoid haunch makes the column flange in the first row of the bolt has a larger stress, as shown in Figure 23-b, with the stress magnitude of 358.78 MPa. At the end of the loading, the beam is also buckling at the location where the first yield of the beam occurs as shown in Figure 23-c. Due to the shape of the haunch, the normal stress of the flange plate is still in the elastic condition with the stress magnitude of 153.92 MPa, as shown in Figure 23-d.

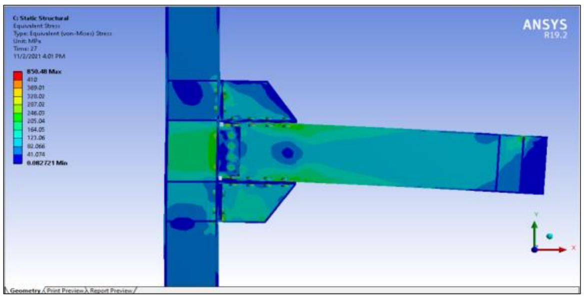

a) Yielding at displacement of 11.1 mm

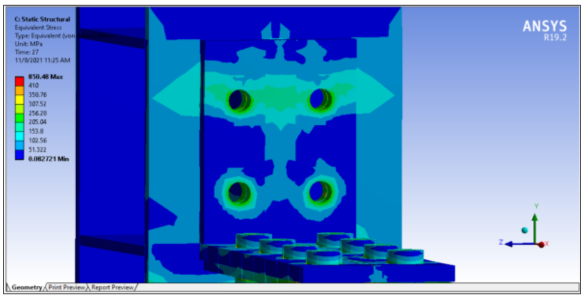

b) Stress on the end-plate at displacement of 11.1 mm

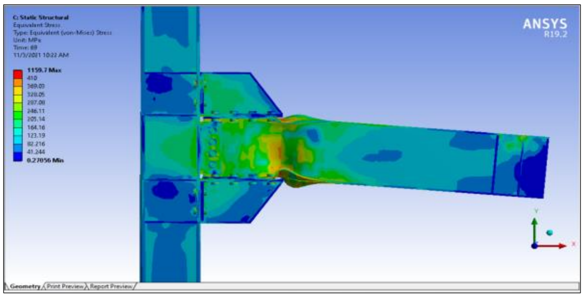

c) Ultimate at displacement of 90 mm

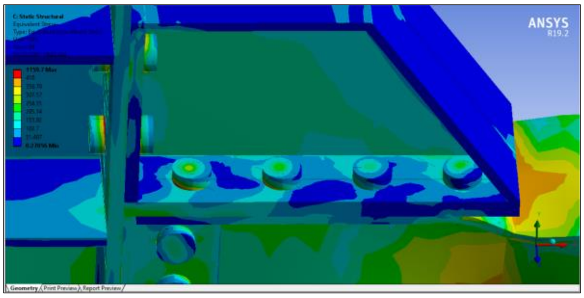

d) Stress on the flange connection at displacement of 90 mm

Figure 23. The von Mises stress of BFP-RTR

e. BFP-RSTR

The moment capacity of the BFP-RSTR model at the face of the column presented in Figure 24. The moment capacity of the connection at rotation of 4% is 206.98 kN-m, as shown in the dot point of Figure 24. The presence of the stiffeners make the moment capacity of the connection increase even though it is not significant, which is an increase of 2.4 kN-m. The prying effect causes a strength degradation due to the insufficient of the end-plate thickness. Therefore, the presence of the stiffeners can prevent the prying effect acting on the end-plate. The maximum moment produced by the BFP-RSTR model is 217.63 kN-m when the rotation occurs at 3.26%. When compared with the plastic moment of the beam, the moment capacity produced by the BFP-RSTR model when the rotation occurs at 4% is still more significant than the plastic moment of the beam. The ratio between the plastic moment of the beam and the connection is 0.836, so the model can meet the prequalification requirements required by the AISC.

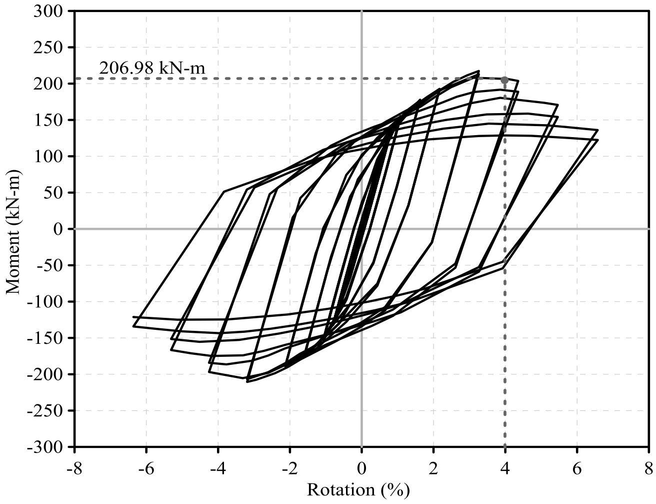

Figure 24. Hysteretic curve of BFP-RSTR model

The von Mises stress of the BFP-RSTR is shown in Figure 25. There is no significant difference between BFP-RTR and BFP-RSTR except that the presence of the stiffener reduced the stress on the haunch web as shown in Figure 25-d, and the end-plate falls into the elastic condition as shown in Figure 25-b. The location of the first yield is the same with the BFP-RTR, which is at the beam flange near the tip of the BFP connection as shown in Figure 25-a. At the end of the loading, the beam is also buckling at the location where the first yield of the beam occurs as shown in Figure 25-c.

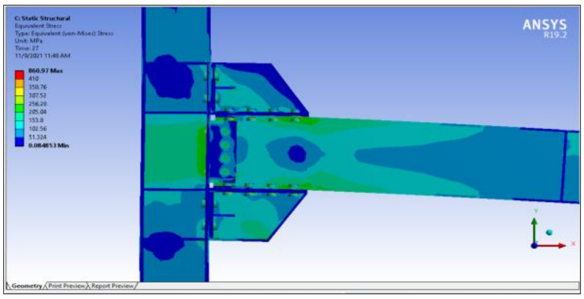

a) Yielding at displacement of 11.28 mm

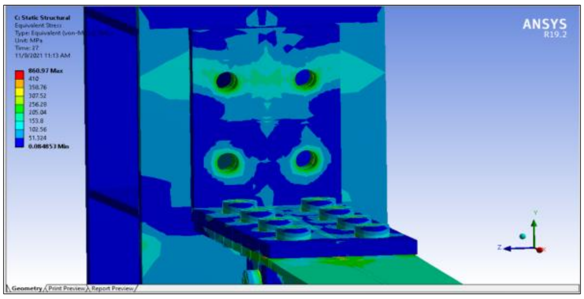

b) Stress on the end-plate at displacement of 11.28 mm

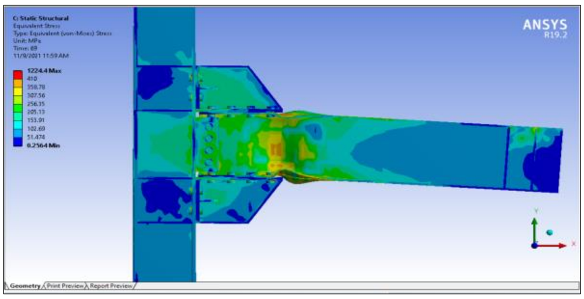

c) Ultimate at displacement of 90 mm

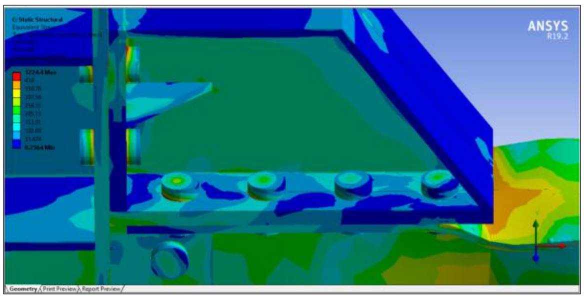

d) Stress on the flange connection at displacement of 90 mm

Figure 25. The von Mises stress of BFP-RSTR

f. BFP-RTRE

The moment-rotation curve of the BFP-RTRE model is shown in Figure 26. The BFP-RTRE model produces a maximum moment of 214.5 kN-m at the rotation of 4.35%, and the curve shows stiffness degradation. When the rotation of 4% occurs, the resulting moment capacity is 214.02 kN-m. The change in bolt geometry from the BFP-RTR model to the BFP-RTRE makes the moment capacity increase by 10 kN-m or an increase of 1.9% from the BFP-RTR model. Compared with 80% of the beam's plastic moment, it will produce a ratio of 0.81. It means that the connection can carry 80% of the beam's plastic moment when there is a rotation of 4%, so that the connection follows the requirements given by AISC.

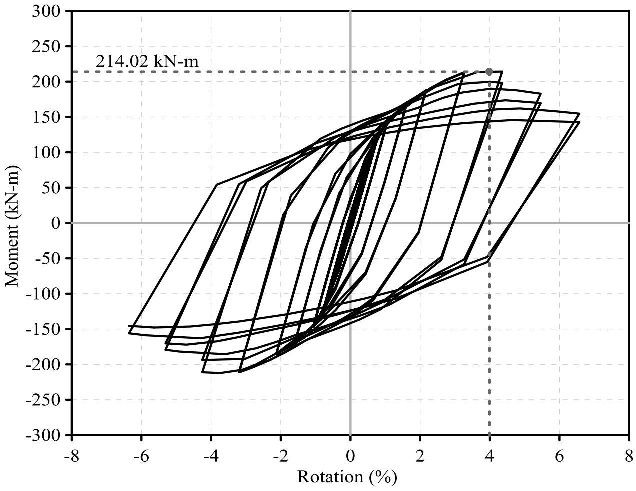

Figure 26. Hysteretic curve of BFP-RTRE model

The von Mises stress of the BFP-RTRE is shown in Figure 27. The first yield of the connection is similar to the BFP-RTR and BFP-RSTR, which is at the beam flange near the tip of the BFP connection as shown in Figure 27-a, with the stress magnitude of 256.28 MPa. However, since the trapezoid haunch has a similar configuration to the extended end-plate, the end-plate yields at the intersection between the haunch flange and the end-plate as shown in Figure 27-b. But since the shape of the haunch is a trapezoid, the prying-effect did not occur and the stress falls into the elastic condition as shown in Figure 27-b. At the end of the loading, the beam is also buckling at the location where the first yield of the beam occurs as shown in Figure 27-c and the flange plate has a slightly stress as shown in Figure 27-d.

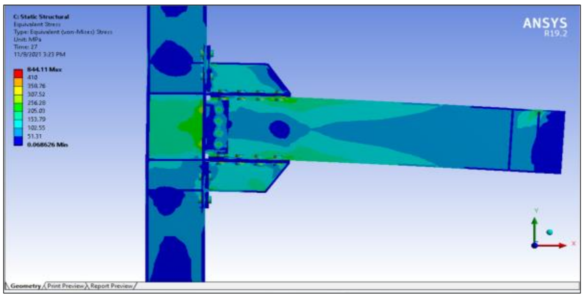

a) Yielding at displacement of 11.28 mm

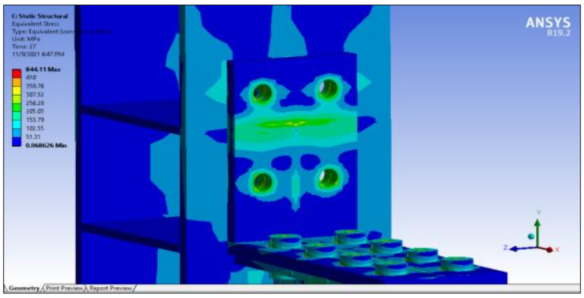

b) Stress on the end-plate at displacement of 11.28 mm

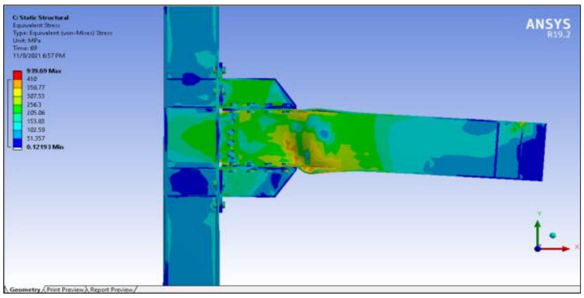

c) Ultimate at displacement of 90 mm

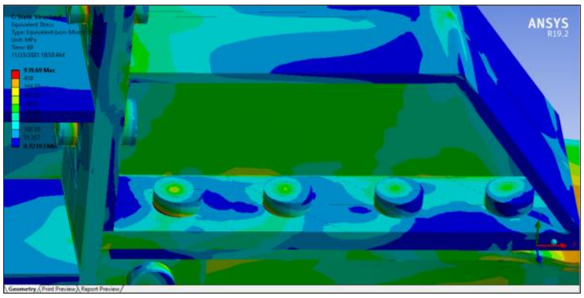

d) Stress on the flange connection at displacement of 90 mm

Figure 27. The von Mises stress of BFP-RTRE

3.3. Comparison of The Moment Capacity and The Backbone Curve of The Connections

The moment capacities of the six connection models are shown in Figure 28. The red line in Figure 28 is the 80% beam's plastic moment, which is 173.16 kN-m. The BFP-UR connection model has the most minuscule moment capacity among the other six models, which is 165.470 kN-m and lower than the red line limit. The retrofitting models using extended end-plates such as BFP-R4E, BFP-R4ES, and BFP-RTRE have relatively the same capacity of 210.667 kN-m, 214.02 kN-m, and 214.018 kN-m, respectively. Those three connections have a moment capacity above 210 kN-m. Meanwhile, the retrofitting model with trapezoidal haunch, namely BFP-RTR and BFP-RSTR, has a moment capacity below 210 kN-m. Each model has a capacity of 204.600 kN-m and 206.980 kN-m

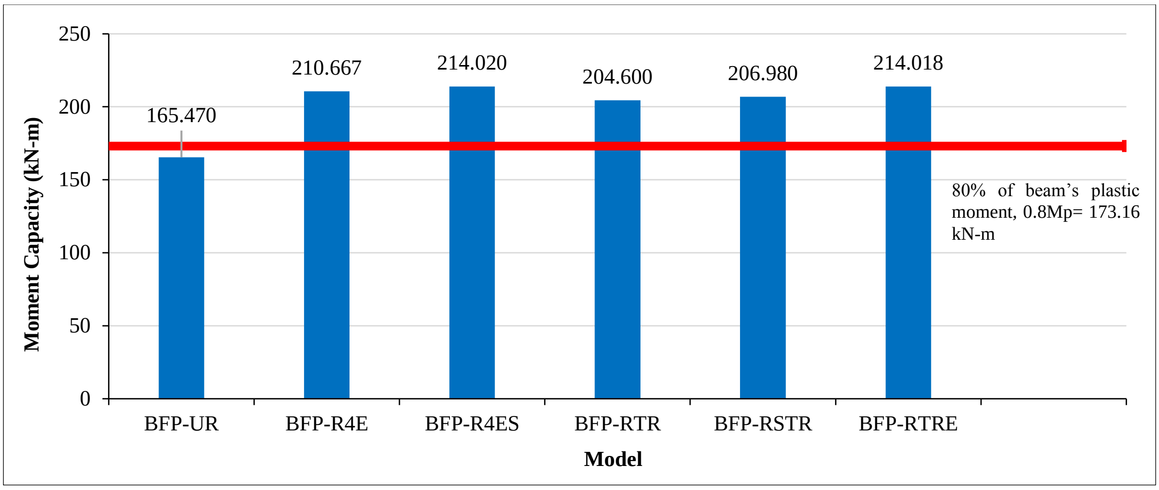

Figure 28. Comparison of moment connection capacity

The variations in bearing capacity observed among BFP connections arise from differences in connection types, the inclusion of horizontal and trapezoidal haunches, the incorporation of extended end plates, and the integration of stiffeners at the end plate. Specifically, the average moment capacity of retrofitting connections fortified with extended end-plate is observed at 212.90 kN-m. Conversely, connections strengthened by trapezoidal haunch exhibit an average moment capacity of 205.79 kN-m. This disparity in moment capacity can be attributed to the positioning of the extended end-plate bolt in close proximity to the compression flange. Consequently, the moment arm of the extended end-plate bolt exceeds that of the bolt utilized in the trapezoidal haunch model, resulting in a longer effective lever arm. Consequently, a retrofitting by using an extended end-plate method yields a greater moment capacity compared to the retrofitting by using trapezoidal haunch.

The normalized moment-rotation curve of the model is presented in Figure 29. The moment strengths are normalized to their maximum moment strengths. All of the models are compared to the BFP-01 conducted by Yilmaz et al. [16], J1.1 conducted by Richards & Lee [9], WHP conducted by Zhang et al. [11], and RS-B-8 conducted by Asada et al. [7]. From the backbone curve, it can be seen that the behavior of the BFP-UR and BFP-01 is almost similar, that is, the pinching behavior is formed due to the slip of bolts at the initial yielding in accordance with the AISC 358-22. From the prespective of normalized moment-rotation curve, the proposed retrofit models have a larger strength and initial stiffness. The proposed model could enhance the strength of the BFP-UR and BFP-0 under large deformation without experiencing failure in the connections or columns. However, the proposed models experienced a gradually stiffness degradation after the rotation of 4% compared to J1.1, WHP, and RS-B-8. Therefore, during the mitigation or evaluation of the connection, a proper haunch dimension should be considered in order to establish a stable curve.

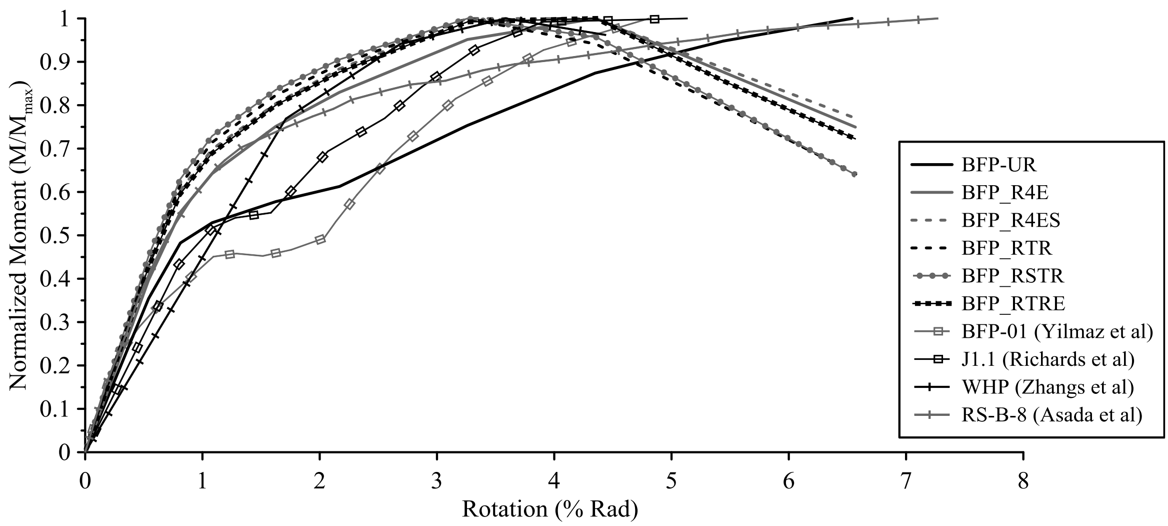

Figure 29. Normalized moment-rotation curve on each moment connection

3.4. Ductility

For a structural member, ductility is the ability to deform in a large deformation without any sudden failure [26-28]. Additionally, it is an important factor in evaluating the behavior whether the member is ductile or not. A structural member with good ductility can control the behavior more and provide more time for emergency response. Generally, the ductility index is defined as a ratio between the ultimate and the first yield deformations [29] and the deformation is obtained from the backbone curve as shown in Figure 29. The first yield deformation, Δ_y, is determined by the reduced stiffness equivalent elasto-plastic yield method [30, 31]. This method was chosen because it is more realistic in calculating the first yield and is suitable for all types of structures. Using the slope obtained by $0.75H_{max}/\Delta H_{max}$, the deformation is linearly extrapolated to the maximum force to determine the yield deformation. The ultimate deformation, Δ_u, is defined as the deformation when the force decreased to 80% of the peak force since a structure have some deformation capacity beyond the peak load without a significant reduction. The definition of the yield and ultimate deformation is illustrated in Figure 30.

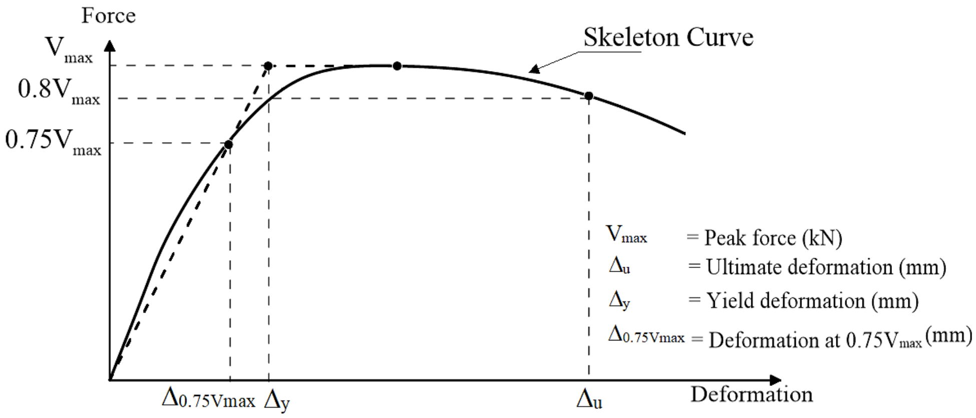

Figure 30. Definition of the yield and ultimate deformation

The ductility of each models is tabulated in Table 4. The BFP-RTR connection model produces the lowest ductility, which is 4.254. Retrofitting with an extended end-plate resulted in an average ductility of 4.845, while reinforcement with a trapezoidal haunch produced an average ductility of 4.31. The ductility produced by the two Retrofitting systems, either strengthened with extended end-plates or trapezoidal haunches, resulted in a good ductility above 4.8. However, the ductility produced by the trapezoidal haunch is 0.535 less than the ductility produced by the extended end-plate.

Table 4. Ductility comparison of finite element result

Model	ϴy	ϴu	Ductility index
BFP-UR	0.909	6.540	7.196
BFP-R4E	1.055	5.294	5.016
BFP-R4ES	1.070	5.149	4.813
BFP-RTR	1.077	4.580	4.254
BFP-RSTR	1.063	4.642	4.366
BFP-RTRE	1.066	5.018	4.707

3.5. Stiffness Degradation

Stiffness is another key criterion for reducing deformation, damage, and providing structural stability [16]. Stiffness can deteriorate owing to cracking, yielding, slip, and buckling [16]. The stiffness degradation may be computed by estimating the secant stiffness per cycle and applying Equation 6 [16].

$$K_i = \frac{|P_i^+| + |P_i^-|}{|\Delta_i^+| + |\Delta_i^-|} \tag{6}$$

where P_i and Δ_i are the peak shear force (kN) and the deformation (mm) of the *i*th hysteretic loop, respectively, and the signs '+' and '-' correspond to the loading direction. The stiffness degradation is normalized to the maximum stiffness and presented in Figure 31.

It can be seen from Figure 31 that the retrofitting models have a quite larger initial stiffness than the BFP-UR. However, when the drift ratio reaches and beyond 3%, the stiffness degradation of the BFP-UR tends to be more stable than the retrofitting model. It can be happened since the beam of the retrofitting model started to yield and buckled at the tip of the Retrofitting area. In contrary, there is no obvious buckling occur in the BFP-UR model but the panel zone has the largest stress. The stiffness of the retrofitting model tends to degrade after the rotation of 2% due to buckling of the beam element. Compared to the BFP-RTR and BFP RSTR, the BFP-RTRE has a similar behavior to the BFP-R4E. It indicates that the combination between trapezoid haunches and extended end-plates could enhance the stiffness degradation.

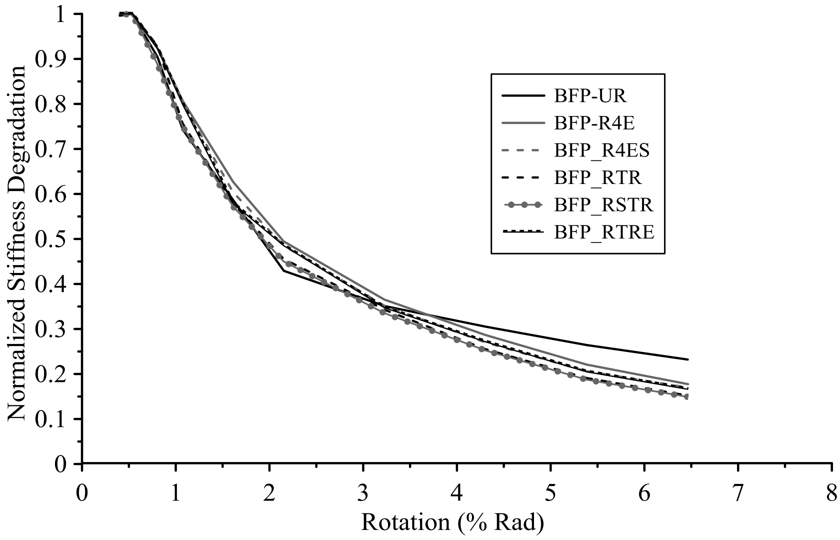

Figure 31. Stiffness Degradation

3.6. Comparison of Energy Dissipation

Energy dissipation is the ability of a structural member to absorb energy under an earthquake, which can be defined by the equivalent viscous damping coefficient ζ_{eq} and cumulative energy dissipation area (E_{sum}) [32]. As described in Figure 32, ζ_{eq} and E_{sum} can be calculated as:

$$\zeta_{eq\_i} = \frac{1}{2\pi}\left(\frac{E_{e+\_i} + E_{e-\_i}}{E_{loop\_i}}\right) \tag{7}$$

$$\mathrm{E}_{sum} = \sum_{i=1}^{n} E_{loop\_i} \tag{8}$$

where E_{e+_i}, and E_{e-_i} are the elastic strain energy for each i cycle, E_{loop_i} is the energy dissipation for each i cycle, and n is the cycle number. The energy dissipation is calculated based on the maximum strength for each cycle.

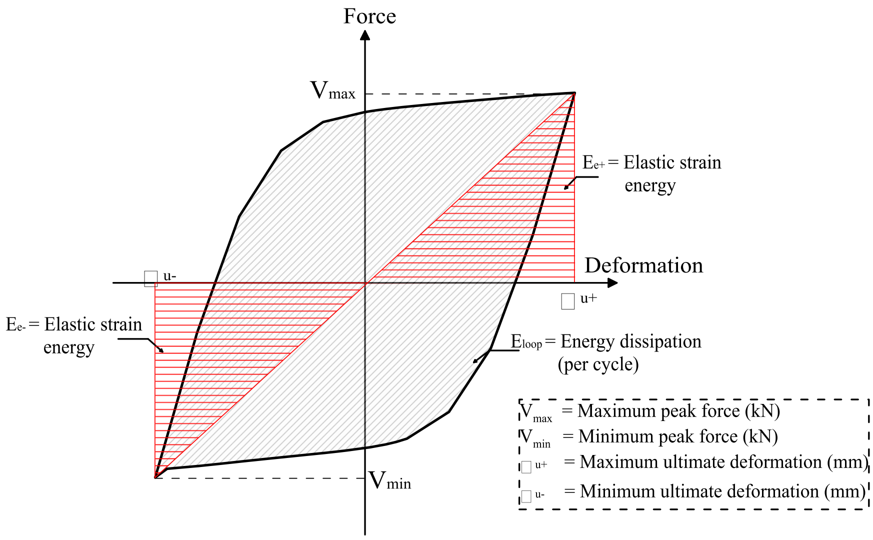

Figure 32. Definition of the equivalent viscous damping equation

Since the BFP-UR has the lowest moment capacity, the energy dissipation produced by the BFP-UR has the lowest trend compares with the Retrofitting model, as shown in Figure 33. At the lower rotation, the energy of all of the connection model is quite similar since steel material has a similar elastic modulus at the elastic condition. However, the difference tends to be huge when the rotation enters in 2%. The BFP-R4ES has the highest energy dissipation, followed by the BFP-R4E because of the moment capacity of the BFP-R4ES and BFP-R4E are bigger than the Retrofitting model with haunch. Moreover, in terms of energy dissipation, the BFP-RTRE has a better performance than the BFP-RTR and BFP-RSTR due to the combination of trapezoid haunches and extended end-plates and the stiffness possessed by the BFP-RTRE.

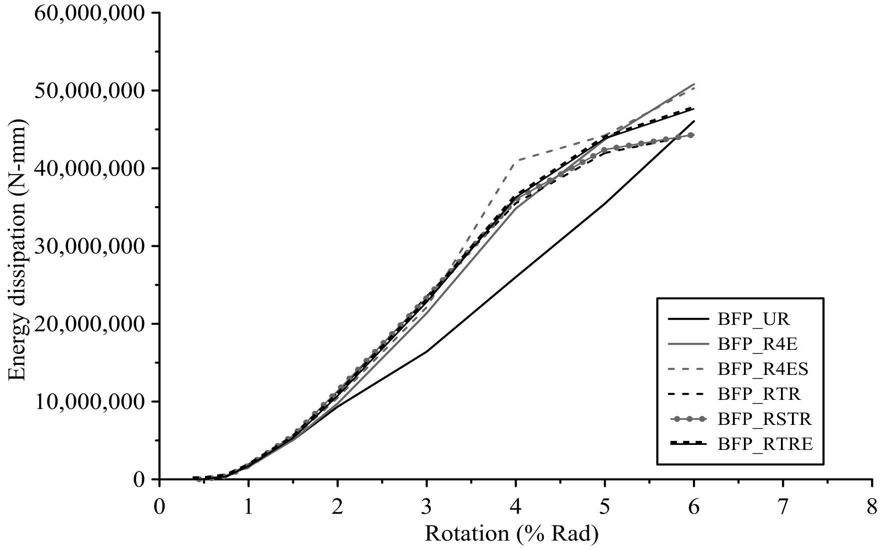

Figure 33. Comparison of energy dissipation

The equivalent viscous damping of each model can be seen in Figure 34. It can be seen that the retrofitting model has a better damping beyond the rotation of 2%. The damping tends to be increasing because of the dissipation area of the retrofitting model is larger than the BFP-UR. Although the BFP-UR has the lowest energy dissipation, the damping ratio of the BFP-UR is larger until the rotation reaches 2%. In terms of equivalent viscous damping, the BFP-RTR and BFP-RSTR have a better damping ratio because both retrofitting models have a larger retrofit area to dampen the stress, although the stiffness of both models is not as stiff as the BFP-RTRE.

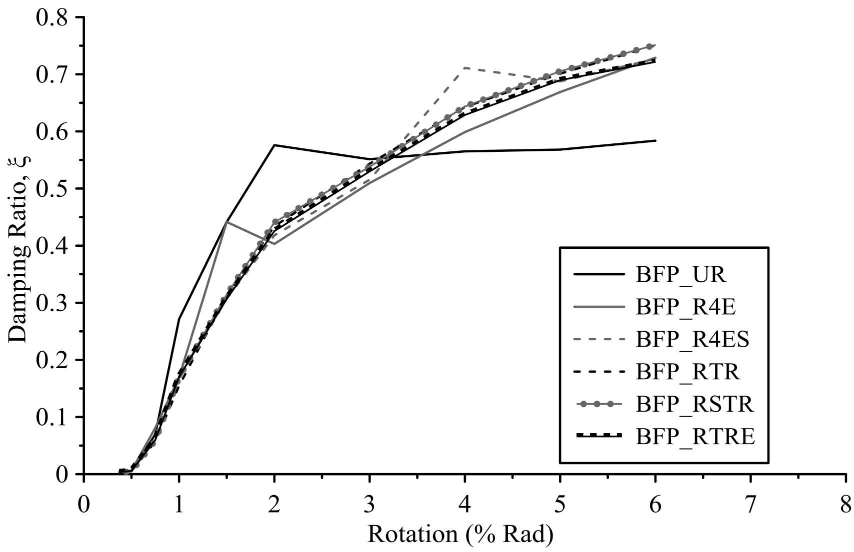

Figure 34. Equivalent viscous damping

4. Conclusions

- Based on the analysis conducted using the ANSYS program, the BFP-UR model demonstrates a rotational moment graph that tends to increase. However, the model encounters a slip phenomenon, evident by a relatively constant moment value when rotation ranges from 1.08% to 1.62%. Consequently, the graph exhibits pinching or a lack of expansion. The Retrofitting models exhibit increased and superior rotational moment graphs compared to the models prior to reinforcement. Nonetheless, they also experience stiffness degradation due to buckling on the main beam. On average, degradation occurs when rotation exceeds 4%. Notably, only the BFP-RTR and BFP-RSTR models displayed degradation after 3% rotation.
- The BFP-UR model, or the existing connection, yields a capacity of 165.47 kN-m when the rotation reaches 4%. In contrast, the BFP-R4E and BFP-R4ES models, which are reinforced by adding an extended end-plate, exhibit moment capacities of 210.667 kN-m and 214.02 kN-m, respectively, at 4% rotation. Additionally, the models with added trapezoidal haunches demonstrate a moment capacity at 4% rotation that is lower than the extended end-plate strengthened connection model.

- The energy dissipation generated by the BFP-UR model amounts to 2,463.454 kN-m-rad, attributed to the absence of stiffness degradation in this model. Meanwhile, the BFP-R4E and BFP-R4ES models exhibit energy dissipation values of 1,864.476 kN-m-rad and 1,899.213 kN-m-rad, respectively. In comparison, the BFP-RTR and BFP-RSTR models yield a lower energy dissipation than the strengthened models with extended end-plates, measuring at 1,186.838 kN-m-rad and 1,194.438 kN-m-rad, respectively.
- Retrofitting the connection proves effective in mitigating the relatively high stress observed in the panel zone area, attributed to the relatively thin thickness of the column web. Retrofitting methods such as the addition of an extended end-plate and the combination of an extended end-plate with a trapezoidal haunch result in an average stress reduction in the panel zone of 37.49% compared to the BFP-UR.

The outcomes of the retrofitting analysis indicate that the connection can withstand 80% of the beam's plastic moment when subjected to a 4% rotation, satisfying the requirements stipulated by AISC 341-16. Among the reinforcement options considered, the BFP-RTRE model, which involves a combined Retrofitting approach using both extended end-plate and trapezoidal haunch, emerges as the optimal choice. This model exhibits a moment capacity higher than that of the strengthened model with trapezoidal haunch alone.

5. Declarations

5.1. Author Contributions

Conceptualization, B.S. and F.G.; methodology, B.S.; software, F.G.; validation, B.S., F.G., and Y.T.; formal analysis, B.S.; investigation, D.I.; resources, B.S.; data curation, B.S.; writing—original draft preparation, B.S.; writing—review and editing, B.S.; visualization, Y.T.; supervision, D.I.; project administration, B.S.; funding acquisition, D.I. All authors have read and agreed to the published version of the manuscript.

5.2. Data Availability Statement

The data presented in this study are available in the article.

5.3. Funding

The authors received no financial support for the research, authorship, and/or publication of this article.

5.4. Conflicts of Interest

The authors declare no conflict of interest.

6. References

[1] Civjan, S. A., Engelhardt, M. D., & Gross, J. L. (2000). Retrofit of Pre-Northridge Moment-Resisting Connections. Journal of Structural Engineering, 126(4), 445–452. doi:10.1061/(asce)0733-9445(2000)126:4(445).

[2] Bruneau, M., Uang, C.-M., & Sabelli, R. (2011). Ductile Design of Steel Structures. McGraw Hill, New York, United States.

[3] Uang, C. M., Bondad, D., & Lee, C. H. (1998). Cyclic performance of haunch repaired steel moment connections: Experimental testing and analytical modeling. Engineering Structures, 20(4–6), 552–561. doi:10.1016/S0141-0296(97)00093-X.

[4] Saberi, H., Kheyroddin, A., & Gerami, M. (2016). Welded haunches for seismic retrofitting of bolted T-stub connections and flexural strengthening of simple connections. Engineering Structures, 129, 31–43. doi:10.1016/j.engstruct.2016.09.050.

[5] Saberi, H., Kheyroddin, A., & Gerami, M. (2017). Seismic strengthening of weak bolted end plate connections using welded haunches. International Journal of Steel Structures, 17(2), 743–755. doi:10.1007/s13296-017-6028-2.

[6] Shi, G., Zhao, H., Chen, X., & Xiao, T. (2020). Experimental study of cyclic behavior of retrofitted beam-to-column joints with welded haunches. Journal of Constructional Steel Research, 171, 106146. doi:10.1016/j.jcsr.2020.106146.

[7] Asada, H., Tanaka, T., Yamada, S., & Matoba, H. (2014). Proposal for seismic retrofit of beam-to-column connection by the addition of H-section haunches to beams using bolt connection. International Journal of Steel Structures, 14(4), 865–871. doi:10.1007/s13296-014-1217-8.

[8] D'Aniello, M., Montuori, R., Nastri, E., Piluso, V., & Todisco, P. (2024). Parametric Finite Element Study on FREEDAM Beam to Column Joints with Different Details of the Haunch Slotted Holes. Applied Sciences (Switzerland), 14(7), 2770. doi:10.3390/app14072770.

[9] Richards, P. W., & Lee, H. (2024). Special moment frame connections with shear-yielding haunches. Engineering Structures, 304. doi:10.1016/j.engstruct.2024.117635.

[10] Sahil, M., Bahrami, A., Waqas, H. A., Amin, F., Mansoor Khan, M., Iqbal, F., Fawad, M., & Najam, F. A. (2024). Seismic performance evaluation of exterior reinforced concrete beam-column connections retrofitted with economical perforated steel haunches. Results in Engineering, 22, 102179. doi:10.1016/j.rineng.2024.102179.

[11] Zhang, Y., Wang, M., & Shi, G. (2024). Mechanical behavior of the extended end-plate connections of a portal frame with various retrofitted constructions under loading. Structures, 63. doi:10.1016/j.istruc.2024.106477.

[12] Qiao, H., Xie, X., Hu, X., Wang, W., & Hong, F. (2024). Experimental study on large deflections of beam–column joints with reinforced flange plates. Journal of Constructional Steel Research, 217. doi:10.1016/j.jcsr.2024.108634.

[13] Sumner, E. A., & Murray, T. M. (2002). Behavior of Extended End-Plate Moment Connections Subject to Cyclic Loading. Journal of Structural Engineering, 128(4), 501–508. doi:10.1061/(asce)0733-9445(2002)128:4(501).

[14] ANSI/AISC 358-16. (2016). Prequalified Connections for Special and Intermediate Steel Moment Frames for Seismic Applications. American Institute of Steel Construction (AISC), Chicago, United States.

[15] Solhmirzaei, A., Tahamouli Roudsari, M., & Hosseini Hashemi, B. (2021). A new detail for the panel zone of beam-to-wide flange column connections with endplate. Structures, 34, 1108–1123. doi:10.1016/j.istruc.2021.08.061.

[16] Yılmaz, O., Bekiroğlu, S., Alemdar, F., Arslan, G., Sevim, B., & Ayvaz, Y. (2019). Experimental investigation of bolted stiffened end-plate and bolted flange-plate connections. Latin American Journal of Solids and Structures, 16(3), e170. doi:10.1590/1679-78255089.

[17] Sato, A., Newell, J. D., & Uang, C.-M. (2008). Cyclic Behavior and Seismic Design of Bolted Flange Plate Steel Moment Connections. Engineering Journal, 45(4), 221–232. doi:10.62913/engj.v45i4.946.

[18] ANSI/AISC 358-22. (2022). Prequalified Connections for Special and Intermediate Steel Moment Frames for Seismic Applications. American Institute of Steel Construction (AISC), Chicago, United States.

[19] ANSI/AISC 341-22. (2022). Seismic Provisions for Structural Steel Buildings. American Institute of Steel Construction (AISC), Chicago, United States.

[20] Kang, H., & Kim, J. (2015). Progressive Collapse of Steel Moment Frames Subjected to Vehicle Impact. Journal of Performance of Constructed Facilities, 29(6), 4014172. doi:10.1061/(asce)cf.1943-5509.0000665.

[21] Kulak, G. (2002). Design guide 17 – High Strength bolts – A Primer for Structural Engineers. American Institute of Steel Construction (AISC), Chicago, United States.

[22] Madenci, E., & Guven, I. (2015). The finite element method and applications in engineering using ANSYS®. Springer, New York, United States.

[23] ANSYS Inc. (2020). ANSYS Fluent Meshing User's Guide. ANSYS Drive, Southpointe, United States.

[24] ANSI/AISC 341-16. (2016). Seismic Provisions for Structural Steel Buildings. American Institute of Steel Construction (AISC), Chicago, United States.

[25] FEMA-350.(2000). Recommended Seismic Design Criteria for New Steel Moment-Frame Buildings. Federal Emergency Management Agency (FEMA), Washington, United States.

[26] Noor, U. A., Jadoon, M. A., Onyelowe, K., Shehzad, A., Ghaedi, K., Alabduljabbar, H., & Javed, M. F. (2024). Non-linear finite element analysis of SFRC beam-column joints under cyclic loading: enhancing ductility and structural integrity. Scientific Reports, 14(1), 18152. doi:10.1038/s41598-024-69270-1.

[27] Fares, A. M., & Bakir, B. B. (2024, July). Parametric study on the flexural behavior of steel fiber reinforced concrete beams utilizing nonlinear finite element analysis. Structures, 65, 106688. doi:10.1016/j.istruc.2024.106688.

[28] Abusafaqa, F. R., Samaaneh, M. A., & Dwaikat, M. B. M. (2022). Improving ductility behavior of sway-special exterior beam-column joint using ultra-high-performance fiber-reinforced concrete. Structures, 36, 979–996. doi:10.1016/j.istruc.2021.12.059.

[29] Zhao, X., Wen, F., Chen, Y., Hu, J., Yang, X., Dai, L., & Cao, S. (2018). Experimental study on the static performance of steel reinforced concrete columns with high encased steel ratios. Structural Design of Tall and Special Buildings, 27(15), e1536. doi:10.1002/tal.1536.

[30] Chen, C. C., Chen, C. C., & Hoang, T. T. (2016). Role of concrete confinement of wide-flange structural steel shape in steel reinforced concrete columns under cyclic loading. Engineering Structures, 110, 79–87. doi:10.1016/j.engstruct.2015.12.002.

[31] Park, R. (1989). Evaluation of ductility of structures and structural assemblages from laboratory testing. Bulletin of the New Zealand Society for Earthquake Engineering, 22(3), 155–166. doi:10.5459/bnzsee.22.3.155-166.

[32] Wang, W., Cai, H., Bai, C., Bao, H., Gao, B., Yuan, Z., & Wang, K. (2023). Seismic performance of partially encased concrete composite columns with corrugated web. Journal of Building Engineering, 77, 107481. doi:10.1016/j.jobe.2023.107481.